Available online at www.sciencedirect.com
SCIENCE DIRECT®
Combustion and Flame 137 (2004) 63–72
Combustion and Flame
www.elsevier.com/locate/jnlabr/cnf

Size-range analysis of diesel soot with ultra-small angle X-ray scattering

Artur Braun,[a,*] Frank E. Huggins,[a] Sönke Seifert,[b] Jan Ilavsky,[c] Naresh Shah,[a] Kerry E. Kelly,[d] Adel Sarofim,[d] and Gerald P. Huffman [a]

[a] *Consortium for Fossil Fuel Sciences, University of Kentucky, Suite 107, Sam Whalen Building, 533 South Limestone Street, Lexington, KY 40506, USA*
[b] *Chemistry and Materials Technology Division, Argonne National Laboratory, Argonne, IL 60439, USA*
[c] *Department of Chemical Engineering, Purdue University, West Lafayette, IN 47907, USA*
[d] *Department of Chemical and Fuels Engineering, University of Utah, Salt Lake City, UT 84112, USA*

Received 22 April 2003; received in revised form 1 December 2003; accepted 1 January 2004

Abstract

Carbonaceous soot produced in a small diesel engine test facility was investigated with ultra-small-angle X-ray scattering. Three soot samples produced using a reference diesel fuel and the reference fuel plus two oxygenate additives were investigated. The presence of objects at three typical size ranges, i.e., aggregates, primary particles, and subunits, was observed. By studying soot powders and pellets from pressed powder, a separation of scattering contributions from aggregates and primary particles was possible. The scattering curves of soot from oxygenated diesel show significant differences between samples obtained under idle and load conditions. Soot from regular diesel fuel did not show such differences.

Keywords: Soot; Combustion; Small-angle; X-ray scattering; Aggregation; Microstructure; Particle size

1. Introduction

Soot from combustion processes has been the subject of uncounted studies for decades and is a continuing topic of investigation. The reasons for studying soot and its formation are manifold:

(i) combustion engineers want to optimize combustion processes to suppress soot formation, because soot may be harmful to materials in engines and furnaces;
(ii) environmental scientists are concerned with soot because of its adverse health effects [1,2] and its possible impacts on global climate [3–5]; and
(iii) the study of the mechanisms of soot formation as a special modification of carbon is of significant fundamental interest.

Particle size is one important structural parameter of soot that is often assessed with microscopy or scattering techniques. Soot particles often occur as fractal aggregates with sizes up to several hundred nanometers, built up from primary particles with sizes of ~ 5–50 nm [6–8]. Knowledge of the aggregate structure is important because many of the physical properties of fractal aggregates may depend on their fractal morphology [9]. It has been found that the primary particles are also built up from subunits, so that typi-

* Corresponding author.
E-mail addresses: artur.braun@alumni.ethz.ch, abraun@lbl.gov (A. Braun).

0010-2180/$ – see front matter
doi:10.1016/j.combustflame.2004.01.003

cally three size ranges are observed. The inclusion of such subunits in primary particles (plerospheres) has been observed before and thus is not a novelty to particles from combustion processes [10].

Ishiguro et al. [11] have observed with transmission electron microscopy (TEM) that diesel soot primary particles contain onion-like subunits. With the same technique, di Stasio [12] reports evidence of three different size scales in soot obtained from an ethylene flame. The early stage of soot inception has been studied recently in flamma using small-angle X-ray scattering (SAXS) [13].

Unlike microscopy, scattering techniques probe the three-dimensional structure and morphology of matter as a bulk technique. This includes light scattering and small angle scattering with X-rays and neutrons. In addition, the fractal dimension can be assessed fairly easily with the latter two techniques. Most small-angle X-ray and neutron scattering facilities at major research laboratories (synchrotron radiation centers and neutron sources) are accessible to qualified personnel of the entire scientific community, based on a competitive proposal rating system, and usually free of charge for nonproprietary research work. Additionally, X-ray tube-based SAXS facilities exist at various universities, not much different from electron microscope facilities.

Small-angle X-ray scattering has extensively been applied to coals and other carbonaceous materials, including carbon black [14] and glassy carbon [15]. Fractal aggregates like carbon black or silica gels exhibit features similar to those of soot and have been studied extensively with SAXS. The early stages of soot inception from gases have been studied in situ with SAXS [13].

Diesel soot is a significant component of fine airborne particulate matter (PM), constituting up to 70% of PM < 2.5 μm in mean diameter in some urban areas. To the best of our knowledge, the present work is the first ex situ SAXS study of soot and the first SAXS study of diesel soot.

2. Experimental procedures

Soot was produced at the diesel test engine facility at the University of Utah from three diesel fuels in a two-stroke diesel test engine (Model Kubota Z482B, 482 cc displacement, typically 0.8–2.2 L/h fuel consumption), operated at 1200 rpm under idle or under load conditions with 10 ft lb and collected on a quartz filter. The fuel/air ratio was 0.013. The engine lubricant was Havoline 10W30 motor oil.

The three diesel fuels included a reference fuel, the reference fuel +5 wt% of diethyl carbonate (DEC; Mix A), and the reference fuel +1.5% DEC + 4.3% ethanol (Mix B). DEC and ethanol served as oxygenates. The diesel was a 50/50 mixture of the Chevron/Phillips reference fuels T-22 and U-15, with an average cetane number of 46.7 and 79 ppm sulfur content. The soot was collected on quartz filters and then separated from the filter for further analyses.

Ultra-small-angle X-ray scattering (USAXS) was carried out using synchrotron radiation at beamline 33-ID at UNICAT, Advanced Photon Source, Argonne National Laboratory. At this beamline, a Bonse–Hart setup allows one to record USAXS scattering curves (SC) using a photodiode detector with an angular resolution of 0.0001 Å^{-1} at a q range from 0.0001 to 1.0 Å^{-1}. The scattering vector q is a typically used quantity in small-angle scattering and relates to the diffraction angle (2Θ), as known from X-ray diffraction, via the relation

$$q = 4\pi/\lambda \cdot \sin\Theta,$$

with X-ray wavelength λ. The data acquisition time for a SC with 150 data points over the q range was typically 15 min per sample.

For SAXS with respect to the large-q tail of the SC, beamline 12-ID at BESSRC-CAT was employed. This beamline has a shorter q range, but a position sensitive detector (CCD camera), which allows one to acquire SC in a shorter time (typically in a fraction of a second). All SAXS and USAXS data were fully corrected for all instrumental effects. The X-ray energies for both experiments were 10,000 eV.

For the SAXS experiments, the soot was evenly distributed on Scotch tape, at a thickness of approximately 200 μm. Since soot is a very good X-ray scatterer at small angles, its scattered intensity dominates the scattering of the Scotch tape by several orders of magnitude, so that this scattering, obtained from a separate reference measurement, could be easily subtracted from the SC of the soot/Scotch-tape assembly as a minor correction. Additionally, pellets of 1 mm thickness and 6 mm diameter were pressed from the soot at a pressure of 3.47 GPa.

Soot powder samples generated with the reference diesel fuel were also measured with a commercial particle sizer. This machine is a combination of a centrifuge (to separate particles) and a laser light beam and detector and applies Stokes' law to determine the sizes of particles immersed in a drop of a liquid [16]. This was a free service provided by CPS Instruments, Inc.

3. Results and discussion

For the basics of small-angle scattering, we refer the reader to the textbook of Glatter and Kratky

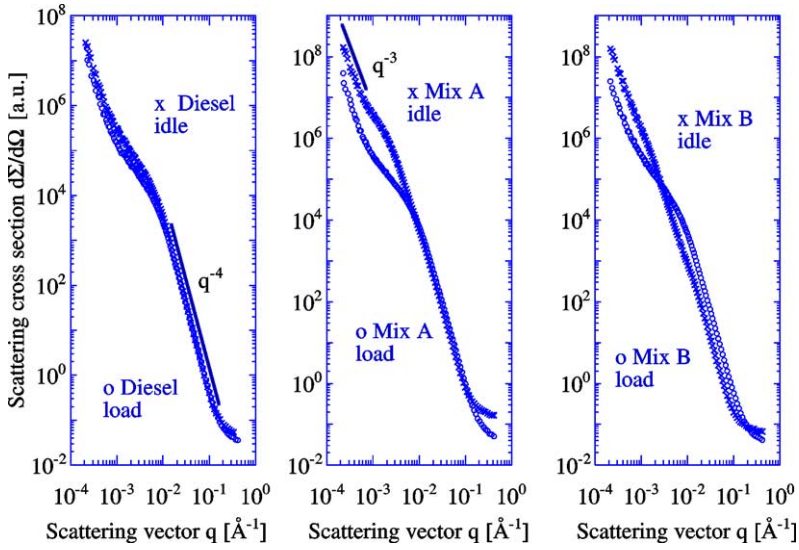

Fig. 1. Log–log plots of scattering curves of powder soot samples.

[17]. Scattering curves of the six soot samples are displayed in Fig. 1.

The ordinate of the plots is the scattering cross section $d\Sigma/d\Omega(q)$, also referred to as the SAXS intensity $I(q)$ in arbitrary units in a typical double logarithmic representation (log–log *plot*). Fig. 1 compares the scattering curves from diesel soot obtained under idle and load conditions from each of the three diesel fuels tested.

Over a q range from 0.0002 to 0.4 Å^{-1}, the scattered intensity varies by 9 orders of magnitude. There is a reciprocal relationship between the q vector and the length L of objects in real space: $L = 2\pi/q$ [17]. With the USAXS setup used here, objects with lengths ranging from 1 nm to 3 μm can be resolved. The drawn straight line in the left plot has an exponent of decay of q^{-4} and serves as a guide to the eye. In the middle plot in Fig. 1, another straight line with q^{-3} also serves as a guide to the eye.

For large q, the intensity shows a straight decay with a power law proportional to q^{-4} for almost all samples studied. After Porod's law [18–20], the q^{-4} decay of the intensity is a confirmation that the soot particles represent a two-phase system (soot particles and the surrounding air or empty space) with a sharp electron-density transition at the particle surface. The hump between $q = 0.001$ and $q = 0.01$ Å^{-1} indicates the presence of a structure with an extension ranging between 60 and 600 nm (large agglomerates or aggregates, built up by primary particles). To the left of this hump, for the lower q, another decay of intensity is observed, however, with a slope less steep than q^{-4}. At the very high q tail, for $q > 0.1$, a constant background causes a bending of the SC, which appears to have a less steep slope in this region. In the further analysis, we will see that an additional structure is present in this region. Generally, however, for both idle and load soot, the SC are very much alike.

The middle plot in Fig. 1 shows the soot from oxygenated diesel (Mix A), for both idle and load conditions. Both SC show a direct overlap in the q^{-4} region, but the bending point for idle is found at a lower q value than that of the load soot, indicating that this structure of soot is larger under idle than under load conditions.

For the soot from Mix B (right plot, Fig. 1), we observe the hump only for the load soot, but not for the idle one.

It turned out that a Kratky plot [21] was most useful to quantify the structure between $q = 0.001$ and 0.01. The Kratky plot is the representation of $I \cdot q^2$ versus q on linear axes, which is very sensitive to the compactness of objects; in particular, compact objects such as spheres exhibit a pronounced maximum in this plot. The position $q_{\max}$ of this maximum is linked with the particle diameter D via $D = \sqrt{2}/q_{\max}$.

Fig. 2 shows the SC in Kratky representation. For better comparison, all curves are plotted on an arbitrary $I \cdot q^2$ scale of similar magnitude. With the exception of the idle sample in Mix B, all SC show an intensity maximum. The idle samples exhibit a maximum at lower q than the load samples, indicating that the scattering objects in this size range (aggregates) are larger when created under idle condition. The sizes of the aggregates from all three fuels under idle and under load condition are summarized in Table 1. The results for Mix B, idle, are obtained from a close inspection of its corresponding log–log plot from Fig. 1, or a log–log representation of its Kratky plot (not shown), which

Table 1
Primary particle and subunit size data obtained from pellet soot and aggregate size data from powder soot

Soot	Subunits		Primary particles			Aggregates D (nm)
	R_g (Å)	D (nm)	R_g (Å)	D (nm)	D (nm)	
Diesel, idle	6.0 ± 0.1	1.5	55.4 ± 2.3	14.3	13.7	29.7 ± 4.0
Diesel, load	6.5 ± 0.2	1.7	39.5 ± 1.0	10.2	11.8	24.2 ± 3.0
NIST 1650	4.9 ± 0.1	1.3	73.6 ± 1.5	19.0	–	19.2 ± 2.1
Mix A, idle	7.4 ± 0.1	1.9	81.8 ± 4.2	21.1	19.4	87.1 ± 14.0
Mix A, load	5.7 ± 0.1	1.5	53.6 ± 1.3	13.8	11.2	24.0 ± 1.7
Mix B, idle	6.5 ± 0.2	1.7	55.3 ± 1.3	14.3	13.0	85 ± 12.8
Mix B, load	6.4 ± 0.1	1.7	85.1 ± 3.7	22.0	14.1	28.7 ± 6.4

Second and third columns show the sizes of subunits, fourth and fifth columns the size of primary particles. The sixth column shows the sizes of primary particles obtained from a Kratky plot. Column 7 shows aggregate sizes obtained from powder samples.

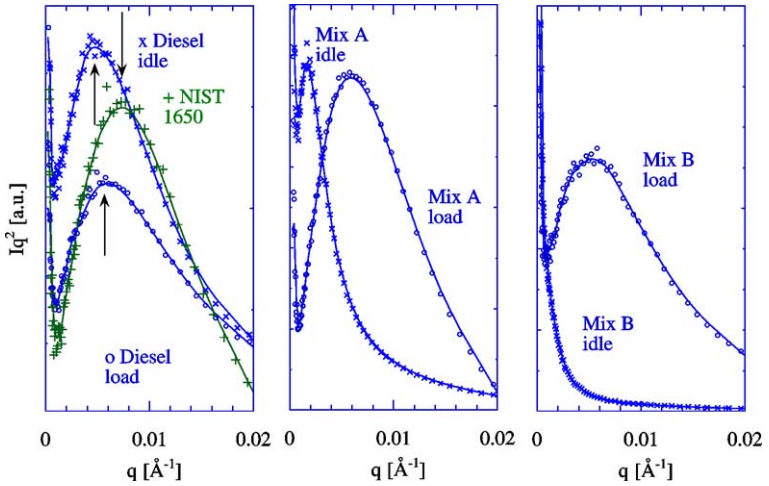

Fig. 2. Kratky plots of the scattering curves of the powder soot samples. Arrows denote where the maximum for particle size determination was assumed.

shows that a structure is present, with a size of approximately 84.7 nm. Some of the maxima in the Kratky plots are rather broad, and they might actually harbor several structures at a time. For instance, closer inspection of the reference diesel soot plots indicates very slight features at $q = 0.0029$ and 0.0025 for idle and load, suggesting aggregates sizes of 49 and 57 nm, respectively. The load samples for Mix A and Mix B show similar, but very weak, signals at 0.0029 and 0.0025 $Å^{-1}$, respectively. The idle samples are very fluffy and possess probably a higher degree of entanglement between the aggregates. Some aggregates may be even larger than those from the load samples. However, these are beyond the detection limit of the USAXS facility, which is 15 µm.

The light scattering results for the idle and load soots from the reference diesel fuel show that aggregates exist with diameters of about 85 nm. Fig. 3 shows the particle number distribution, $P(R)$, of these samples. We have fitted a log normal distribution to the data points in order to determine the mean radius, R_0, and the width, σ, of this distribution:

$$P(r) = \frac{1}{\sqrt{2\pi}} \frac{1}{R\,\sigma} \exp\left(-\frac{ln^2\, R/R_0}{2\sigma^2} \right). \quad (1)$$

These sizes of 85 nm for reference diesel soot are not found with SAXS; but SAXS shows that particles of such size exist in the idle soot of Mix A and Mix B. We point out that the particles in the light scattering experiments were immersed in liquids, and this might have an effect on the aggregates' size.

Another structure is present at approximately $q = 0.01$ $Å^{-1}$. This structure, which is almost hidden and very hard to make out in the Kratky plots of the powder samples (Fig. 3), becomes much more obvious in the pellet samples. The Kratky plots of the SC from the pellet samples are displayed in Fig. 4. All load samples have pronounced and clear maxima in their intensity, at q values of approximately 0.01 $Å^{-1}$. It is noteworthy that the reference diesel idle and load

soots show very similar SC with sharp intensity maxima. However, the maxima for the idle samples from Mix A and Mix B are less pronounced than those for the load samples.

Remarkably, the structure observed at the very small q for the powder samples due to aggregates vanishes in the SC of the pellet samples. The structures now visible in the SC of the pellets are most likely the primary soot particles with a size of about 10 to 20 nm. This finding is supported by transmission electron microscopy results, as displayed in Fig. 5. Pressing soot into pellets is thus a technical trick to remove the aggregate structure, which otherwise overshadows the scattering signature of the primary particles. The current methodology for soot primary particle size determination is through analysis of TEM micrographs, but recently, laser-induced incandescence [22] was successfully applied to the same task.

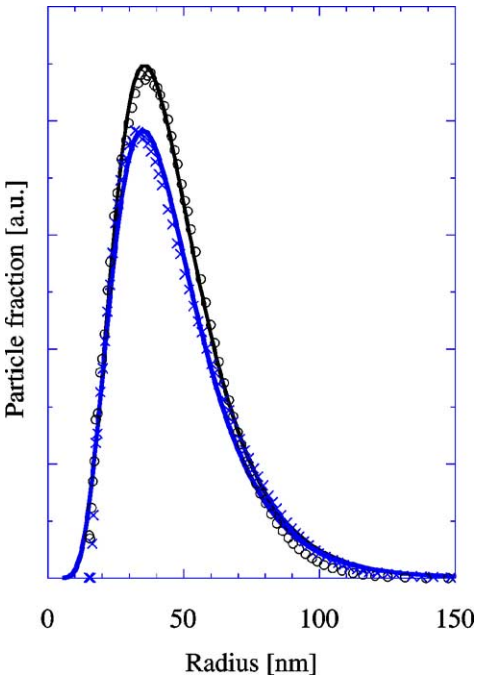

Fig. 3. Particle size distribution for soot from the reference diesel fuel (×, idle; ○, load), as obtained from light scattering of powder. The solid line is the least-squares fit of the data points to a log normal distribution (Eq. (1)).

Our TEM results show that the primary soot particles are globules with diameters of around 20 nm. The high-magnification TEM micrographs also show the previously reported [11] onion-like subunits, which are incorporated in the primary particles. Those have a mean size of about 5 nm and are not easily discerned in the raw SAXS scattering curves, since particles this small will scatter only at $q \sim 0.1$ Å^{-1}. To investigate structures in the high q range, further analysis of the SC is required, as illustrated in Fig. 6.

All SC became subject to more specific analysis at the high q range for $q > 0.01$. The circular data points represent the original SC, and the dashed line is a least-squares fit of Eq. (2) to the SC:

$$I(q) = c_1 + c_2 \cdot q^{-4}. \tag{2}$$

This is the relation for the so-called Porod scattering of objects with smooth surfaces or interfaces in a two-phase system [18–20]. By subtracting this Porod scattering fit curve from the original data, we can isolate the scattering due to the objects of very small size. The fit curve was subtracted from the SC, and the result is the modified SC indicated by open circles in Fig. 6. The pronounced shoulder in this modified SC

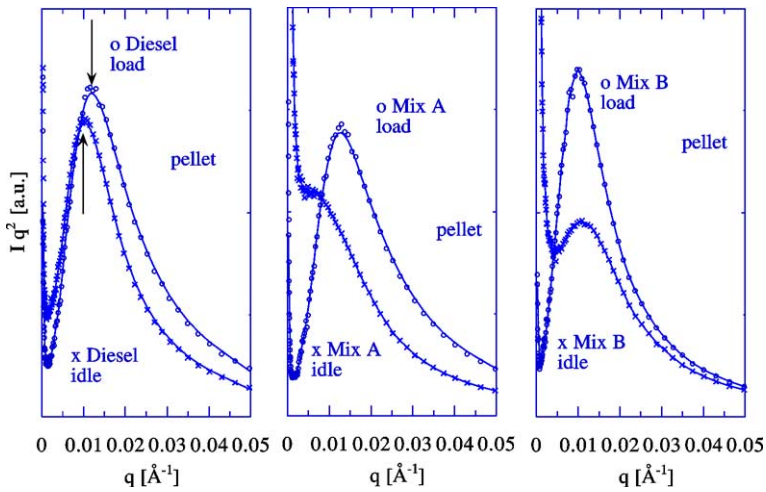

Fig. 4. Kratky plots of the scattering curves of the pellet soot samples. Arrows denote where the maximum for particle size determination was assumed.

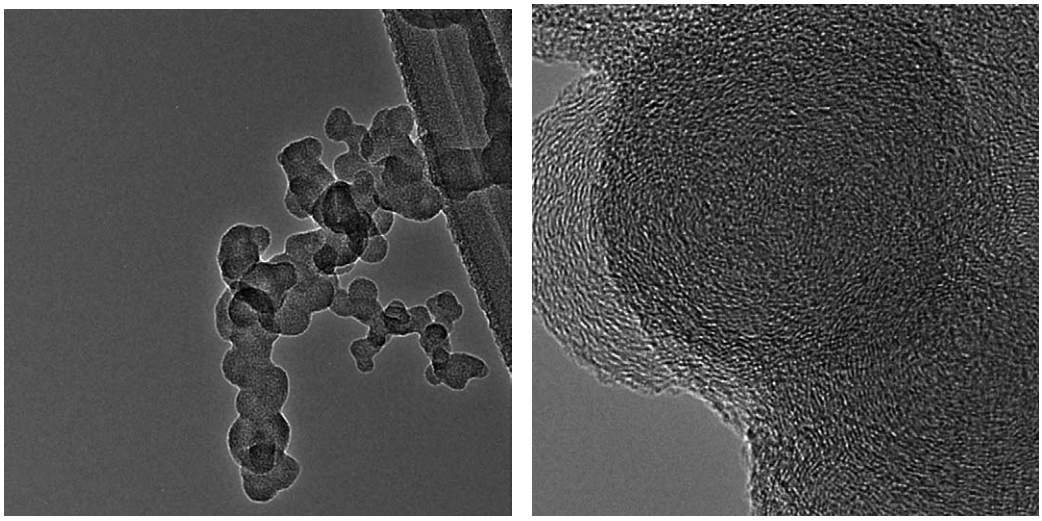

Fig. 5. TEM micrographs of soot particles. Left: An agglomerate. Right: A primary particle.

in the q range from 0.2 to 0.5 indicates the presence of a structure with a size of about 10 Å. We applied a Guinier fit [17,23] to this modified SC, which is the solid line that intercepts with the intensity axis at $q \approx 0.3$:

$$I(q) = NV^2 \Delta n_f^2 \cdot \exp\left(-\frac{q^2 R_g^2}{3}\right). \tag{3}$$

N is the number of particles in the irradiated sample volume, detected in this q range; V is the volume of a single particle; and Δn_f^2 is the X-ray scattering contrast between the particles and their environment.

R_g is the radius of gyration of the objects, which is the mean square distance from the center of electron density of a particle (in analogy to the momentum of inertia in mechanics),

$$R_g^2 = \frac{\int_V \rho(r_i) r_i^2 \, dV}{\int_V \rho(r_i) \, dV}, \tag{4}$$

with ρ being the number of electrons per unit volume in the sample.

From the least-squares fit of Eq. (3) to the Porod-subtracted SC, we find a radius of gyration of 5.95 Å for the structure at high q. The same procedure was applied to the structure at $q \approx 0.02$; here, we find $R_g = 55.40$ Å. The drawn line, with intercept at about 100 on the intensity axis, represents the corresponding fit (Fig. 6). Almost all objects with some geometrical regularity can be assigned a structure factor [17]; this is a function of q vector and a geometrical parameter of the object such as the radius for a sphere, or the length of the axes of a prism, or an ellipsoid, and so on. Guinier has found that for the central part of the scattering curve, a universal approximation exists for all particle shapes with the radius of gyration as

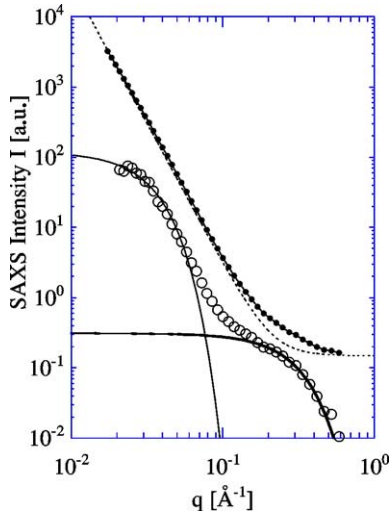

Fig. 6. SC from diesel idle pellet sample (filled data points) and least-squares fit with Porod's law (dotted line, after Eq. (2)). Data curve with open symbols is the difference between two former curves, including two least-squares Guinier fits after Eq. (3).

the only parameter (Eq. (3)). There exist conversion formulae that transform R_g into the geometrical parameter mentioned. The relationship between the radius R of a sphere and R_g is, for instance,

$$R = \sqrt{\frac{5}{3}} R_g. \tag{5}$$

Unless indicated otherwise by supplemental experimental evidence, the assumption of sphere-like structures is often justified. In the present case, the Guinier analysis of our data indicates sphere-like objects with dimensions of approximately 1.5 to

14.3 nm. It should be noted, however, that Guinier's approximation actually holds only for dilute systems. Soot powders and pellets may be considered a dense system and a rigorous analysis would require a particle–particle correlation function as additional correction. We have not included this correction and the particle sizes determined may therefore be somewhat overestimated. Size data are summarized in Table 1.

Our results are supported by high-magnification TEM. The right TEM image of Fig. 5 is typical of the structure of our diesel soot observed at high magnification. Indeed, we observe that there are abundant onion-like subunits made that have diameters ranging from approximately 2 to 20 nm. These onion-like structures are made from parallel graphene sheets arranged with their basal planes perpendicular to the radii of the structures. Ishiguro et al. [11] have observed similar structures in diesel soot and di Stasio [12] makes similar observations on soot from a Bunsen burner fed by ethylene.

The observation that the graphene sheet planes are perpendicular to the radii of the primary particles finds its manifestation in another SAXS observation. In Fig. 1 we find that the exponent of decay for $q > 0.01$ is close to 4 for all soot samples studied here, indicating that the system obeys Porod's law. With the perpendicular arrangement, there is a sharp electron-density transition between graphene planes and empty space. The opposite case would not provide such a sharp transition and would yield a smaller exponent of decay [24]. The pellets show a smaller exponent of decay than the powder samples.

In a number of recent publications about carbon black, deviations from Porod's law, i.e., a noninteger exponent of decay at high q values, had been erroneously attributed to fractal characteristics of the material [25]. Such fractal characteristics, however, may be apparent only because misalignment of graphene sheets, which is typical for many disordered carbons, would cause a scattering contribution, which together with Porod scattering would infer a noninteger exponent of decay [25]. In our samples, at high q values, we observe that Porod's law is well maintained. For the powder samples, the exponent of decay is higher than 3.8 in every case and usually close to 4. For the pellet soot samples, the exponents of decay are somewhat smaller, but not lower than 3.77. This might be due to the fact that in pellets, the primary particles are closer together and thus the assumption of a sharp electron-density transition between particle and empty space does not hold anymore. The exponents of decay are summarized in Table 2 for comparison.

One anonymous referee of this paper has raised the question whether the small structures at very high q might be caused by so-called micropores, for instance. In fact, assuming that soot is basically some graphite-like material, it should have a theoretical mass density of 2.268 g/cm^3 (the upper limit). The presence of pores would cause a lower mass density, though. To account for this pore effect, one can introduce the skeleton density, or X-ray density, which is obtained from the (002) Bragg reflex position in the case of carbonaceous materials.

Deviations of the (002) peak position from the (002) reference peak of graphite, i.e., a peak shift toward smaller diffraction angles, are then interpreted as wider spacing of the corresponding Bragg planes and thus a smaller density than graphite. The (002) peak positions of our soot samples ranged from 23.87° to 24.45° for 2Θ.

From the position of the (002) peak (Θ_{002}) in the X-ray diffractogram, the layer distance d_{002} was determined using the Bragg equation:

$$\lambda = 2 \cdot d_{002} \cdot \sin \Theta_{002}. \tag{6}$$

The density ρ_x of the soot can then be calculated from X-ray data according to [26],

$$\rho_x = (3.33538/d_{002}) \times 2.268 \text{ g/cm}^3, \tag{7}$$

where 2.268 g/cm^3 is the density of graphite with $d_{002} = 3.33538$ Å.

The skeleton density ρ_x of our soot samples thus did not exceed 2.03 g/cm^3. Our soot pellets, however, had an apparent mass density ρ_g not exceeding 1.2 g/cm^3.

Table 2
Exponent of decay for all soot samples in the long and short q range

Fuel	High q, powder	High q, pellet	Low q, powder	Low q, pellet
Diesel, idle	3.99	3.89	3.28	2.89
Diesel, load	3.86	3.86	3.12	3.16
NIST 1650	4.00	3.86	3.12	2.46
Mix A, idle	3.97	3.77	3.02	3.36
Mix A, load	3.96	3.94	3.09	3.45
Mix B, idle	3.92	3.80	2.96	3.39
Mix B, load	3.98	3.95	2.75	2.80

The absolute error for the exponent is better than 0.02.

We determined the porosity p of the soot from its X-ray density ρ_x and its apparent density ρ_g, which can be obtained from the weight and the dimensions of the sample, by using the relation [26]

$$p = 1 - \frac{\rho_g}{\rho_x} \tag{8}$$

and found a value of $p \approx 41\%$.

This porosity can be caused by pores and voids of various sizes. The fact that we press the primary particles close together when we press pellets reveals that some degree of porosity is maintained between these particles. We have no direct information, however, that a microporosity is present in the primary particles. However, we believe that the TEM micrographs of soot look quite similar to TEM micrographs of glassy carbon [27,28]. Glassy carbon (GC) is a carbon material synthesized by pyrolysis of phenolic resins and has a very high internal surface area due to pronounced microporosity. The micropores can be as small as 1 nm, and the internal surface area ranges from 1000 to 2000 m^2/g, at mass densities around 1.5 g/cm^3. The pores have to be considered as voids because they have no connectivity. TEM does not allow for a direct visualization of these pores. Instead, the porosity of GC is believed to be enclosed in polyhedra built up by graphene sheets. GC has been extensively studied with SAXS and shows structural features at very high q, which are attributed to the micropores. However, it is not possible to tell the micropores and the nanocrystallites apart in a scattering experiment, because they basically have a similar size. Only recently an attempt was made to show that the typical small-angle scattering of glassy carbon in the high q range is due to the voids and not due to the graphite-like crystallites. But this was an indirect approach and involved an oxidative treatment (activation), which opens and interconnects the voids and then has particular impacts on the evolution of the small-angle scattering correlation function [29].

Fig. 7 compares the SAXS curves of the NIST reference soot sample (curve with open circles) and SAXS curves of three types of GC. The most typical scattering feature of GC is the intensity plateau for $q < 0.2$ $Å^{-1}$ and the Guinier range right next to this plateau, toward higher q values. The lower scattering curve (filled squares) is from a 60-μm-thick GC sample, pyrolyzed at 1000 °C, and with radius of gyration 7.8 Å. The two shorter SAXS curves are unpublished data with absolute intensity calibration ($cm^2/(cm^3$ srad)), obtained from two 1-mm-thick GC samples pyrolyzed at 1000 °C (K-type, solid line) and 2200 °C (G-type, dotted line), at Hamburger Synchrotronstrahlungslabor, JUSISA SAXS facility (Hamburg, Germany). The corresponding radii of gyration are 5.7 and 9.2 Å, respectively. These radii

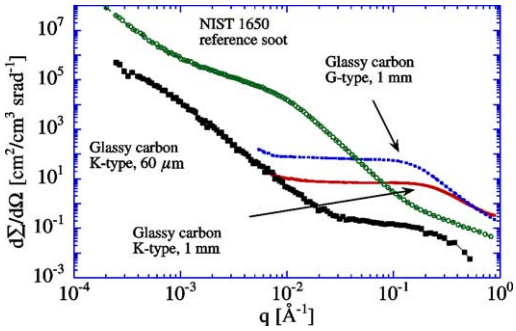

Fig. 7. SC of NIST 1650 reference soot sample (open symbols) and glassy carbon plates with 60-μm (filled symbols) and 1-mm-thickness. Solid line is from K-type GC, pyrolyzed at 1000 °C, dotted line is from G-type GC, pyrolyzed at 2200 °C.

were obtained from the Guinier ranges near 0.15 and 0.2 $Å^{-1}$, respectively. The subunits of the soot particles are basically found in the same q range. The power law exponent of decay in this q range is very close to 4 for the soot samples, in line with Porod's law. This holds not for the GC samples, for which we observe exponents around 2.5. It remains therefore open whether the primary particles and subunits contain a microporosity that would account for the relatively low mass density. Possible experimental routes to test soot for microporosity could include oxidative treatment, i.e., thermochemical [15] or electrochemical [30] activation, with subsequent gas adsorption analysis or double-layer capacity measurement. Such a route would be advisable because preliminary work on soot oxidation has already been performed [31].

It is not always possible to decompose structural information such as power laws or humps that arise from objects, in particular when the structure is as complex as in the present case. Pressing particles together in pellets is found useful because the aggregates' structure is altered, and therefore this structural feature can be identified more easily against other structures in the SAXS curve. We have applied Guinier fits to the load diesel pellet sample in this region and found an aggregate diameter of 39 nm, while on the corresponding powder, 77 nm was found. For the load Mix A pellet it was 29 nm, and 72 nm for powder. For load Mix B, the diameter was 45 and 98 nm for the pellet and powder, respectively. We thus are assured that the feature in this q range can be attributed to aggregates with diameters of about ~ 80 nm.

4. Conclusions

We have investigated soot powders and pellets with small-angle X-ray scattering and found three characteristic size ranges. The most prominent feature

is visible in the log–log plot of scattering curves between $q = 0.001$ and 0.01 $Å^{-1}$, which is due to soot particle aggregates. This feature is altered by pressing the powder into pellets. The original aggregate size ranges between 70 and 100 nm and thus is comparable to results based on laser light scattering and other published work on diesel soot. Additional, finer features were found in a range of the SC that obeyed Porod's law. Subtraction of Porod scattering contributions gave access to these finer structures, which were identified as the primary particles (10–20 nm diameter) and subunits (1.7 ± 0.2 nm) of these particles. These structures are believed to be onion-like structures of graphene sheets that are seen in high-magnification TEM images and range in size from approximately 2 to 20 nm.

In summary, a methodology has been developed for analysis of SAXS data obtained from diesel soots that is capable of distinguishing three primary size parameters that characterize the soot: a soot particle aggregate size, a primary particulate size, and a particulate subunit size. For the current samples, the aggregate size ranged between 70 and 100 nm, the primary particulate size was typically 10–20 nm, and the particulate subunit size was approximately 2 nm. These results are consistent with transmission electron microscopy results obtained by our group and by others [11,12]. Although the TEM results are more easily interpreted and illustrative than SAXS, the SAXS measurement has the advantage of being much less time consuming, requiring only minutes per sample, while TEM may require hours or even days for a complete investigation of a sample. Additionally, the SAXS method has the advantage of being a bulk measurement that yields results characteristic of and statistically significant for the whole sample, while TEM by its nature can probe only a minute amount of the total sample. It therefore seems logical that these two methods should be used for structural analysis in a complementary manner, with SAXS providing high-throughput screening for large numbers of soot samples and TEM examining the more interesting samples in more detail.

Acknowledgments

Support for this research under National Science Foundation (NSF) CRAEMS Grant CHE-0089133 is gratefully acknowledged. We are grateful to Ron Ellis (CPS Instruments, Inc., Stuart, FL, USA) for the light scattering experiments. SAXS was performed at BESSRC-CAT, and USAXS was performed at the UNICAT facility at the Advanced Photon Source (APS), which is supported by the University of Illinois at Urbana–Champaign, Materials Research Laboratory (US DOE, the State of Illinois–IBHE–HECA, and the NSF); the Oak Ridge National Laboratory (US DOE under contract with UT–Battelle LLC); the National Institute of Standards and Technology (US Department of Commerce); and UOP LLC. The APS is operated by the University of Chicago for the US Department of Energy, Basic Energy Sciences, Office of Science under Contract W-31-109-ENG-38. SAXS data on two GC samples were collected (A. Braun, 1998) at Hamburger Synchrotronstrahlungslabor, JUSIFA SAXS facility, Hamburg, Germany, with financial support from the board of the Swiss Federal Institute of Technology (ETH Zürich), within the Swiss Priority Program on Materials Research, by the Paul Scherrer Institute, Villigen, Switzerland.

References

[1] D.W. Dockery, J. Schwartz, J.D. Spengler, Environ. Res. 59 (1992) 362–373.
[2] Third External Review Draft of Air Quality Criteria for Particulate Matter, April 2, 2002; US Environmental Protection Agency, Washington, DC, 2002.
[3] M.Z. Jacobson, J. Geophys. Res. 106 (2001) 1551–1568.
[4] D. Koch, J. Geophys. Res. 106 (2001) 20311–20332.
[5] W.L. Chameides, M. Bergin, Science 297 (2002) 2214–2215.
[6] R.A. Dobbins, R.A. Fletcher, H.-C. Chang, Combust. Flame 115 (1998) 285–298.
[7] L.A. Sgro, G. Baseile, A.C. Barone, A. D'Anna, P. Minutolo, A. Borghese, A. D'Alessio, Chemosphere 51 (2003) 1079–1090.
[8] A.C. Barone, A. D'Alession, A. D'Anna, Combust. Flame 132 (2003) 181–187.
[9] A.V. Filippov, M. Zurita, D.E. Rossner, J. Colloid Interface Sci. 229 (2000) 261–273.
[10] C. Allouis, F. Beretta, A. D'Alessio, Chemosphere 51 (2003) 1091–1096.
[11] T. Ishiguro, Y. Takatori, K. Akihama, Combust. Flame 108 (1997) 231–234.
[12] S. di Stasio, Carbon 39 (2001) 109–118.
[13] J.P. Hessler, S. Seifert, R.E. Winans, T.H. Fletcher, Faraday Discuss. 119 (2001) 395–407.
[14] T. Rieker, S. Misono, F. Ehrburger-Dolle, Langmuir 15 (1999) 914–917.
[15] A. Braun, M. Bärtsch, B. Schnyder, R. Kötz, O. Haas, H.-G. Haubold, G. Goerigk, J. Non-Cryst. Solids 260 (1999) 1–14.
[16] CPS Instruments, Inc., Stuart, FL, USA.
[17] O. Glatter, O. Kratky, Small-Angle X-ray Scattering, Academic Press, New York, 1982.
[18] G. Porod, Kolloid-Z. 124 (1951) 83–114.
[19] G. Porod, Kolloid-Z. 125 (1952) 51–57.
[20] G. Porod, Kolloid-Z. 125 (1952) 109–122.
[21] Kratky Plot. IUPAC Compendium of Chemical Terminology, second ed., 1997.
[22] R.L. Vander Wal, T.M. Ticich, A.B. Stephens, Combust. Flame 116 (1999) 291–296.

[23] A. Guinier, Ann. Phys. 12 (1939) 161.

[24] R. Perret, W. Ruland, J. Appl. Crystallogr. 1 (1968) 308–313.

[25] W. Ruland, Carbon 39 (2001) 323–324.

[26] A. Gupta, I.R. Harrison, J. Lahijani, J. Appl. Crystallogr. 27 (1994) 627.

[27] V.A. Drits, T. Tchoubar, X-ray Diffraction by Disordered Lamellar Structures, Springer-Verlag, Berlin, 1990.

[28] G.M. Jenkins, K. Kawamura, Polymeric Carbons—Carbon Fibre, Glass and Char, first ed., Cambridge Univ. Press, Cambridge, UK, 1976.

[29] W. Gille, A. Braun, J. Non-Cryst. Solids 321 (2003) 89–95.

[30] A. Braun, J. Kohlbrecher, M. Bärtsch, B. Schnyder, R. Kötz, O. Haas, A. Wokaun, Electrochimica Acta 49 (2004) 1105–1112.

[31] R.L. Vander Wal, A.J. Tomasek, Combust. Flame 134 (2003) 1–9.